ISSN: 2162-5786 Vol. 5, No. 1, March 2015

Scientific Research Publishing

Open Journal of Acoustics

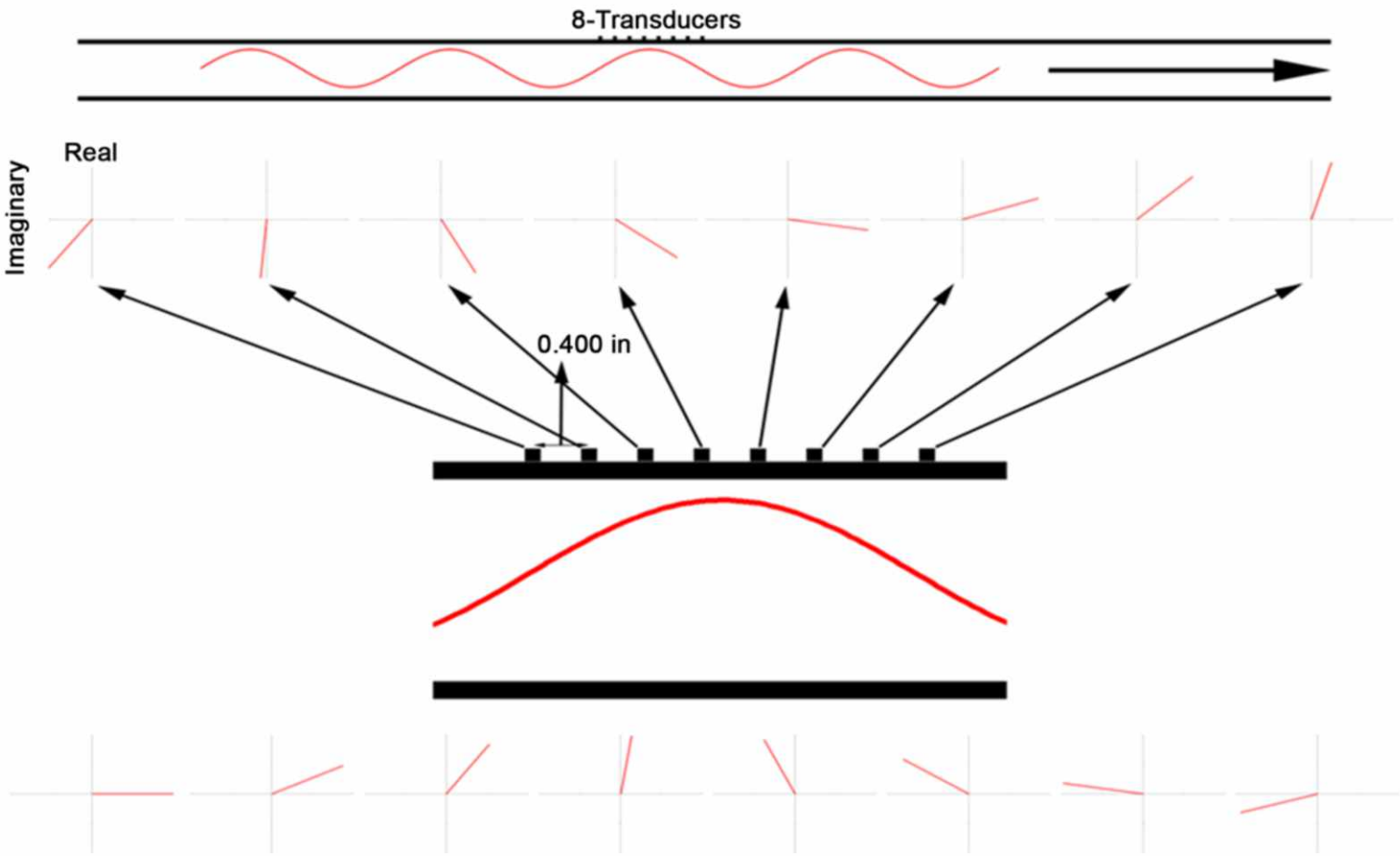

ISSN:2162-5786

www.scirp.org/journal/oja

Journal Editorial Board

ISSN 2162-5786 (Print) ISSN 2162-5794 (Online)
http://www.scirp.org/journal/oja

Editor-in-Chief

Editorial Board

Open Journal of Acoustics, 2015, 5, 1-28
Published Online March 2015 in SciRes. http://www.scirp.org/journal/oja

Table of Contents

Volume 5 Number 1 March 2015

The figure on the front cover is from the article published in Open Journal of Acoustics, 2015, Vol. 5, No. 1, pp. 25-28 by Ken McGill, Kathryn Harke and Kris Schock.

Open Journal of Acoustics (OJA)

Journal Information

SUBSCRIPTIONS

The *Open Journal of Acoustics* (Online at Scientific Research Publishing, www.SciRP.org) is published quarterly by Scientific Research Publishing, Inc., USA.

Subscription rates:

Print: $79 per issue.
To subscribe, please contact Journals Subscriptions Department, E-mail: sub@scirp.org

SERVICES

Advertisements
Advertisement Sales Department, E-mail: service@scirp.org

Reprints (minimum quantity 100 copies)
Reprints Co-ordinator, Scientific Research Publishing, Inc., USA.
E-mail: sub@scirp.org

COPYRIGHT

PRODUCTION INFORMATION

For manuscripts that have been accepted for publication, please contact:
E-mail: oja@scirp.org

Open Journal of Acoustics, 2015, 5, 1-10
Published Online March 2015 in SciRes. http://www.scirp.org/journal/oja
http://dx.doi.org/10.4236/oja.2015.51001

Noise Annoyance Due to Wind Flow Interaction with a Building's Facade

Marcos Raul Lisboa, José Cataldo Ottieri, Alice Elizabeth González

IMFIA, Faculty of Engineering, University of the Republic, Montevideo, Uruguay
Email: mlisboa@fing.edu.uy, jcataldo@fing.edu.uy, elizabet@fing.edu.uy

Received 15 January 2015; accepted 3 March 2015; published 5 March 2015

Abstract

The analysis of acoustic emissions generated by the interaction between the wind and a building's facade of approximately 90 m high, located in the city of Montevideo, is presented. There is a helipad on the roof of the building. It is surrounded by a perforated plate (4.87 m high). Once the building was finished, complaints about the noise annoyance were expressed by some neighbors and working population in the building. Measurements of sound pressure levels on the site have been done. Also the possible acoustic sources were physically characterized. The noise source was identified: the acoustical emissions were associated with a phenomenon caused by wind speeds above 20 m/s from different directions, generating high sounds pressure levels in octave band of 4000 Hz, after its passage through the perforated plate on the contour of the roof. These studies were complemented by measurements in wind tunnel using a physical model built with the same plate installed in the building, which allowed verifying the results.

Keywords

Noise Annoyance, Wind, Building, Perforated Plate

1. Introduction

The sound results from a propagation of an oscillatory movement of particles through a material medium, which has associated an oscillatory field of pressures. Such movement and oscillatory field of pressures can be associated to different processes such as vibration of a solid surface, implosion or explosion of steam bubbles or oscillations of flow due to the occurrence of instabilities, among others. Once the oscillatory field is produced, the resulting propagation velocity will be characteristic of the medium in which it is developed, known as speed of sound. The sound produced is then characterized by frequency and amplitude of oscillatory motion.

The aforementioned sound wave is associated to a flow of power per unit area that surrounds the site where

the source generates such movement. Integrating the power flow on a surface surrounding, the issuer is possible to estimate the emitted power, which is often expressed as power level in decibels (dB).

This paper presents the analysis of acoustic emissions generated by the interaction between the wind and the facade of a building. Indeed, according to the complaints of the people living and/or working in the area around the building, the occurrence of certain weather events generated noise emissions with such intensity to be heard; they may result in a potential cause of discomfort or annoyance, constituting the events of interest.

Consequently, a physical characterization of possible sound sources in the building was made. The sound production process was physically described, and its frequency and intensity were estimated. In addition, a set of measurements were developed to characterize the sound that was registered in areas of interest of the building, particularly on the roof of it. The results were verified by wind tunnel tests of the faculty of engineering. Finally, a diagnosis was made and mitigation actions were proposed.

2. Characteristics of the Noise Source

2.1. Building Description

The tower under study is part of a special architectural complex that comprises several buildings with similar characteristics. The site where the tower is located is presented at different scales in **Figure 1**.

In **Figure 1(d)**, the building under consideration is indicated by the star. Also, a building 120 m high that is located between the SOUTHWEST and SOUTH-SOUTHWEST directions relative to it indicated by a circle.

The building under study, **Figure 2(a)**, is something more than 88 m high. The floor of the roof is placed at 81 m over the ground; it is surrounded by a parapet built of masonry 1.6 m high. Over it, an open window of 0.82 m over the top edge of the guardrail is defined all along the perimeter, just to the lower edge of a perforated metal plate 4.87 m high, that is supported by vertical tubes. A helipad is located at the center of the roof [1].

The plate at the top of the building is a plate of Aluzinc 0.5 mm thick. It has four segments on each face, **Figure 2(b)**: two of them are 5.24 m wide and the others are 6.26 m wide; all of them are 4.87 m high. It has horizontal folds every 4 cm, conferring to it a trapezoidal appearance as shown in **Figure 2(c)**. The supports are vertical tubes of rectangular cross-section of 50 mm by 100 mm and 4.87 m high.

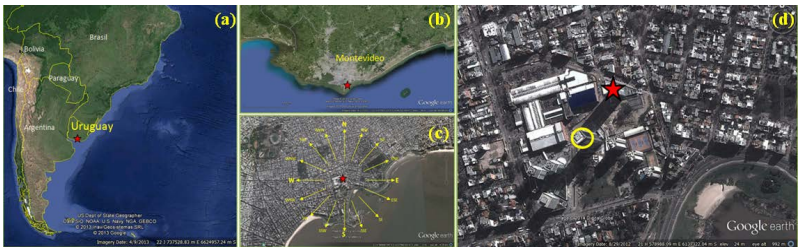

Figure 1. Location of the study site, on a continental scale (a); Department-wide Montevideo (b); City, where the location according to the cardinal points (c) is included; and (d), in the building complex (images modified from Google Earth).

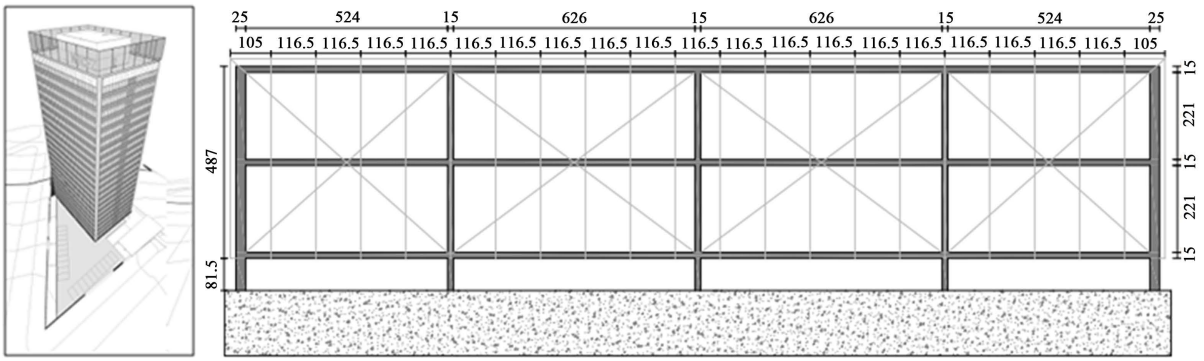

(a) (b)

Figure 2. (a) Sketch of the building under study. Elevation of a plate; (b) Front view; (c) Court (reproduced from [1]).

The plate is a perforated plate with circular holes arranged in rows. The diameter of the holes is 2.5 mm, the gap between holes in each row is 5 mm and the spacing between rows is also 5 mm.

Two cooling towers of the air conditioning system are installed on the roof, in the free space around the heliport, as well as pumps and fans associated with their operation. Also, some impulses in the area of the ventilation system are identified. Some other discharges of the ventilation system are located close to the level of the street.

2.2. Possible Sources of Acoustic Emissions

Many building sites where potentially annoying acoustic emissions may occur were identified. They are presented and discussed on next sections.

Flow around the structure

The interaction between air flow and a structure can result on vortex shedding with a scale similar to dimensions of the structure [2]. These vortexes are emitted with a characteristic frequency, depending on the geometry of the obstacle and that is directly related to the velocity of the incident flow over the obstacle. A fluctuating pressure field results, and an acoustic emission is induced.

If D is the width of the obstacle, U is the mean value of the incoming wind speed and f is the vortex shedding frequency, the Strouhal number is set to [3]-[5] as:

$$St = \frac{f \cdot D}{U} \tag{1}$$

In this case, this parameter has a value of about 0.12 for the building [6]. Taking into account that the width of the building is 23 m, the emission frequency of vortices for a wind speed of 20 m/s would be less than 1 Hz. Lower wind speeds also lead to lower frequencies.

Acoustic emissions in support tubes

If conditions are established for a fluctuating flow to occur inside the tubes that support the perforated plate, e.g. a speed change of the wind that slips around the pipes, these tubes can become noise sources. Depending on the boundary conditions, e.g. an open end and a closed one, the induced sound wave becomes stationary and it remains moving inside the tube.

The frequency of the wave depends on the length of the tube and on the speed of the waves. For ideal gases, as it can be assumed that the air behaves in this case, this speed is temperature dependent.

The frequency of pressure waves and their velocity were determined from the analysis of non-stationary flow inside a tube [7], for air temperature of 15˚C. The frequency was found to be about 35 Hz.

Vibration of the perforated plate

The air flow around the plates results turbulent. Then a fluctuating load onto the shields presents a non-stationary response and therefore a vibration is induced on them by the same wind action.

To characterize the effects of turbulent wind velocity component, v' turbulence intensity I as used:

$$I = \frac{\sqrt{\langle v'^2 \rangle}}{U} \tag{2}$$

At the height of the plate where the shed is located turbulence intensity would be 0.25.

In particular, the fluctuating components of velocity having a frequency corresponding to the first normal mode of vibration of the plate are very significance. To calculate the frequency of that mode, each shield was examined as a set of homogeneous bar recessed or projecting both ends as appropriate. Each bar or shield portion between consecutive supports, has a mass of approximately 11.5 kg, being the modulus of elasticity of 72 GPa. The frequency of the first vibration mode of the shield portion at both ends embedded would be 117 Hz, while the cantilever frequency of the present a first normal mode of 177 Hz. Anyway this frequency induces a fluctuating pressure field and therefore the acoustic signal output.

On the roof, the movement of each leg shield induces a level of sound pressure of the order of 38 dBZ. Since total would be about 80 sections of sheet metal and assuming all sections emit sound, the sound pressure level on the floor of the roof of the building—if there was no obstacle to propagation- would be of the order of 44 dBZ in while scale A would be approximately 33 dBA.

Flow through the holes

When the wind flows around the building is set up a pressure field on its envelope[1]. If P is the gauge pressure at a point of the shell and U is the mean wind speed at the height of the building, the pressure coefficient according to the following expression is defined [4]:

$$C_p = \frac{P}{\frac{1}{2}\rho U^2} \tag{3}$$

The pressure differences which are set up on the sides of the building generate a flow through the orifices and across the free span between the shield and the parapet roof (slot). These flows attempt to detach the boundary layer with vortices generation (jet flow around) with a geometrical scale similar to the hole and slot dimension *i.e.* 2.5 mm and 0.82 m respectively.

The frequency of shedding of the vortices and its sound intensity level will depend on the wind speed.

The resistance to the flow through the holes is slightly higher compared to that presented for the slot. For example, for a value of average wind speed of about 20 m/s, the air velocity in the slot is about 16 m/s, while it is about 12 m/s in the holes. In this case, the flow of vortices around the slot would present a frequency of 19 Hz, while vortices emitted by the holes would have a frequency about 4800 Hz. Each hole is assumed to be an acoustic transmitter on this frequency.

The characteristic frequencies and sound pressure levels for an average wind speed of 20 m/s at the building height, for each one of the major characterized emitters are presented in **Table 1**.

3. Field Measurements

For sound pressure levels (SPL) characterization, three long-term continuous monitoring campaigns were performed on the roof. Additionally, other manual measurements of sound pressure levels and velocity measurements at the site were taken, to characterize the possible sound sources, and registered events of interest (see **Table 2**). For the identification of the events to be studied, it was assumed that the occurrence of sound events was linked to high wind velocity events simultaneously occurring with complaints about noise annoyance from people who work in the tower or from inhabitants of the close neighborhood.

Table 1. Characteristics of major acoustic sources.

Issuer	Frequency (Hz)	L (dBZ)
Flow around the building	1	-
Support tubes	35	74.0
Vibration plate	177	44.0
Flow through the slot	19	-
Flow through the holes	4800	83.4

Table 2. Measurements of sound pressure levels taken at the study site.

Noise Measurements	Duration
Long term measurements	
M1—first monitoring	11 days
M2—second monitoring	9 days
M3—third Monitoring	17 days
Short term measurements	
MP1—characterization of sound sources, environmental measurements	4 hours
MP2—building roof measurements and event of interest during	2 hours

[1]Fields of pressures would be established on the building for various wind directions were derived from testing in small scale model made in the wind tunnel of the faculty of engineering [1].

Four main measuring points were established on the roof of the building, thus covering four areas defined by their geometry, **Figure 3**.

Continuous measurements for long-term SPL were taken with a sound meter Casella CEL 633-C, Class 1 according to IEC 61672. The instrument was located at point 4 on all three occasions (M1, M2, and M3). For short-term manual noise measurements (MP1 and MP2) a B&K 2250 sound level meter, Class 1 according to IEC 61672 was used. Both instruments have current calibration and certification by traceable laboratory according to international standards.

For analyze events of interest, wind data registered from National Ports Administration (ANP, for its acronym in Spanish), were used. ANP monitors wind speed and direction each 1 minute. The anemometer is located 30 m over the level of the ground and a distance of 6.5 km to the WEST of building site.

On the other hand, for the analysis of wind climate in the studied area, a historical data series of hourly average wind speeds from Carrasco Weather Station was used. Carrasco Station has an anemometer installed at 10 m relative to the ground elevation. It is located about 12 km to the NORTHEAST of the point of interest.

In a complementary way, and in a particular case, wind measurements in the study site were made with a portable Anemometer Extech brand, model EN300.

Noise

Based on the whole information obtained from long- and short-term measurements of SPL, sound emission events associated with wind-induced flow through the facade of the building, were identified for the studying period.

The following information is summarized in **Table 3**:

-The time of occurrence of the event of interest;

-The frequency of identified pure tones and their sound pressure level relative to the average SPL of both lateral third-octave bands;

-The speed and wind direction at the height of the roof, assuming that it is the cause of noise emissions.

As it can be seen in **Table 3**, wind noise emissions were associated with a strong high-pitched sound which is perceived as a ringing on the roof. It is a strong pure tone at frequencies identified as belonging to the 4000 Hz octave-band [8]. Note that the superelevation of these tones is 17 dBZ above the sound pressure levels on their sidebands in 6 of the 27 events identified and in all but one case are greater than 10 dBZ. Sound pressure levels exceeding 90 dBZ were measured on the roof. These emissions would cause annoyance, because they would be perceived as annoying as broadband sound of (LA + 6) dBA [9] intensity because of their frequency and intensity (LA is intended to be the sound pressure level of the real broadband sound).

Features of the Events of Interest

From short-term measurements

During the performance of MP2, the occurrence of sound events that could be potential causes of annoyance was verified. Sound emissions were detected when the wind speed at the rooftop was expected to exceed from

Figure 3. Points of sound measurements in the roof.

Table 3. Events of interest identified on the building roof.

Measurement	Time	Frequency Pure Tone (Hz)	Sound Pressure Levels		Wind[a]	
			Pure Tone (dBZ)	Superelevation of the Tone (dBZ)	Speed (m/s)	Direction
MP2	3:58:49 PM	5000	86.5	12	19.0	WSW
M2-day 1	3:41:00 PM	3200	92.0	17	19.5	NE
M2-day 1	3:49:00 PM	3200	91.4	16	16.0	ENE
M2-day 1	3:54:00 PM	3200	80.7	12	17.8	ENE
M2-day 6	11:28:00 PM	3200	87.4	14	32.3	ESE
M2-day 6	11:29:00 PM	3200	85.1	13	32.3	ESE
M2-day 6	11:32:00 PM	3200	83.9	13	18.0	ESE
M2-day 6	11:41:00 PM	3200	84.7	11	19.5	ESE
M2-day 7	5:20:00 AM	3200	88.3	16	29.1	SSE
M2-day 7	5:21:00 AM	3200	85.2	16	29.1	SSE
M2-day 7	5:26:00 AM	3200	87.9	16	20.8	S
M2-day 7	5:27:00 AM	3200	90.0	17	29.1	SSE
M2-day 7	5:28:00 AM	3200	88.1	16	25.1	SSE
M2-day 7	5:31:00 AM	3200	80.2	14	22.0	S
M2-day 7	5:32:00 AM	3200	85.6	15	30.4	SSE
M2-day 7	5:34:00 AM	3200	92.0	17	25.1	SSE
M2-day 7	5:35:00 AM	3200	86.2	16	16.0	SSE
M2-day 7	5:37:00 AM	3200	84	15	26.4	SSE
M2-day 7	5:39:00 AM	3200	85.2	16	22.0	SSE
M2-day 7	5:40:00 AM	4000	88.4	4	30.4	SSE
M2-day 7	5:41:00 AM	3200	86.5	16	20.8	SSE
M2-day 7	5:46:00 AM	3200	84.5	16	34.7	SSE
M2-day 7	6:00:00 AM	3200	81.8	15	27.6	SSE
M2-day 7	6:27:00 AM	3200	85.5	15	26.4	SSE
M2-day 7	6:28:00 AM	3200	89.8	17	27.6	SSE
M2-day 7	6:29:00 AM	3200	92.3	17	23.6	SSE
M2-day 7	6:30:00 AM	3200	91.2	17	27.6	SSE
M2-day 7	6:31:00 AM	3200	81.1	14	26.4	SSE

16 m/s, blowing from WEST-SOUTHWEST direction. The flow through the perforated plate was the cause of the measured sounds.

In **Figure 4** the features of one of the studied events are presented. It was identified at the SPL time evolution for a 16 minutes sample (**Figure 4(a)**). The spectral composition of a one minute sample of noise including the signal of interest is shown at **Figure 4(b)**.

From long-term measurements

The spectra of some studied events are presented in **Table 3**. They are also graphically described in **Figure 5**.

The spectra of the analyzed events have a similar shape: they have lower intensities on low frequencies, then a

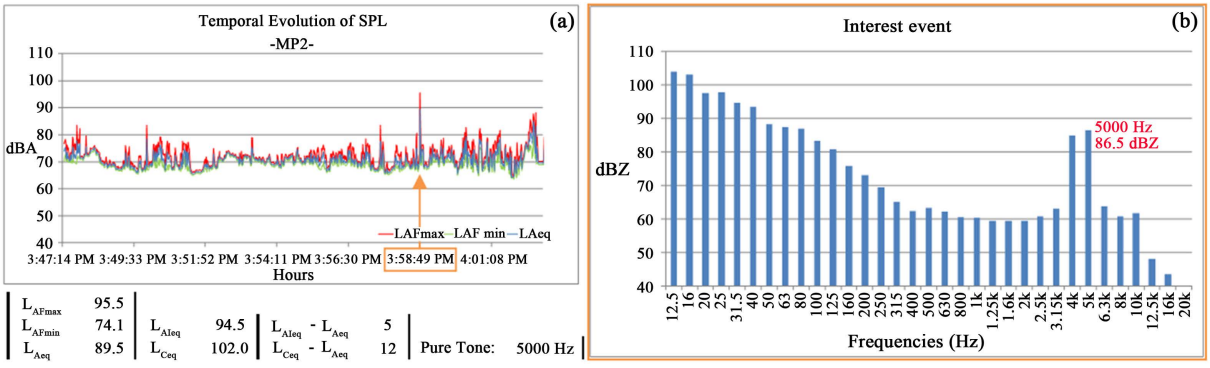

Figure 4. Description of the event of interest measured. (a) Evolution of SPL; (b) Spectral composition.

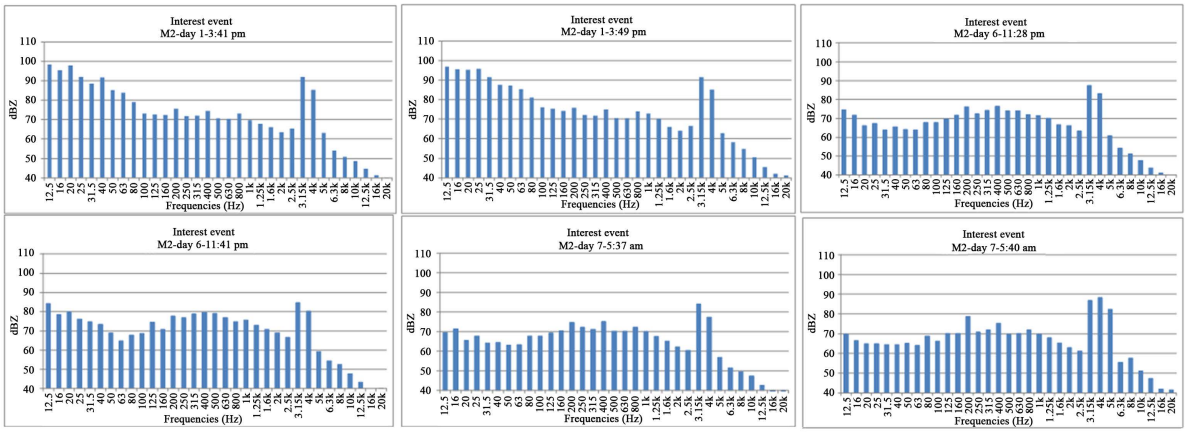

Figure 5. Spectral composition measured SPL event interest.

peak in midrange and another lower zone towards the high frequencies region where the above mentioned pure tones [8] can be found.

4. Wind Tunnel Test

In order to verify the behavior of the perforated plate as an acoustic source, a test was conducted in a wind tunnel of the faculty of engineering, UdelaR. At its entrance a flow straightener honeycomb consisting of hexagonal cross-section tubes of 26 mm side and a free passing area of 86.2% of the total area is located. To represent the shield under study, a perforated plate was placed 1.31 m downstream of the entrance of the tunnel. In **Figure 6** a sketch of that wind tunnel and your work area is shown.

SPL measurements with two Class 1 sound level meters were performed simultaneously both inside and outside of the tunnel. A sound level meter B&K 2250 was located in the center of the straight section, 3.43 m downstream of the entrance of the tunnel, and another Class 1 sound level meter Casella CEL-633C was installed out of the wind tunnel, 2 m downstream of its exit. The air velocity close to the microphone of the sound level meter outside the wind tunnel was measured with a handheld anemometer Extech EN300.

Two tests were carried out in two different working conditions. In the initial one, called basic condition, the test was conducted without the perforated plate, to determine the base noise. In the second condition the plate is installed. For each operating condition of the fan and for each test situation, the frequency of the identified pure tone and its sound pressure level measured inside the wind tunnel, in dBZ, are presented in **Table 4**.

The longitudinal turbulence intensity current above the shield was 2%, whereas the longitudinal integral scale of the turbulence was 5 mm [1].

For each speed of the wind tunnel fan, the speed of the air flow through the orifices and the value of the characteristic frequency of the acoustic emission were estimated, as shown in **Table 5**. Note that the obtained frequency values are similar to those determined at the field measurements (**Table 4**). **Table 5** presents an estima-

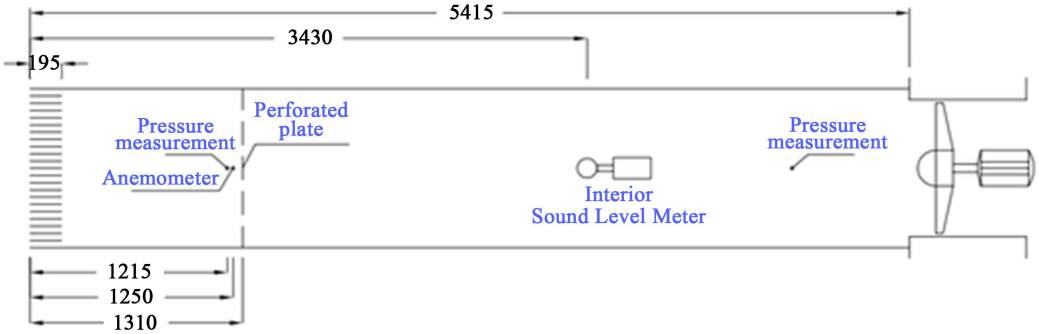

Figure 6. Sketch of wind tunnel.

Table 4. Frequency of pure tones for different fan rotation speeds.

Imposed frequency regulator frequency (Hz)	Speed fan (RPM)	Pure tone frequency (Hz)	L (dBZ)	
			Base noise	Perforated plate[a]
30	600	2000	79.8	-
		2500	-	64.6
40	800	3150	89.4	69.0
50	1000	4000	93.5	71.3
60	1200	5000	96.7	72.3
70	1400	6300	103.3	72.8

[a]The energy associated with the base condition has just been subtracted in the informed levels.

Table 5. Frequency deduced from the air speed in hole.

Imposed frequency regulator frequency (Hz)	V_{hole} (m/s)	Frequency (Hz)	L (dBZ)
30	7.6	3030	77.8
40	9.9	3957	81.7
50	12.1	4838	86.6
60	14.3	5723	89.1
70	15.5	6197	90.5

tion of the sound intensity level, assuming that each hole can be intended as an acoustic monopole, as it was done to obtain the values presented at **Table 1**.

Even if the estimated sound pressure levels are higher than measured ones, they follow a similar pattern (**Table 5**). Levels increase when so does the velocity of the air flow through the holes; this was also observed in some of the measurements in the wind tunnel.

Taking into account the theoretical developments presented, the results of field and wind tunnel measurements, it should be inferred that acoustic emissions on the roof of the building are due to the wind flow through the holes in the perforated plate installed as a shield over the building.

To evaluate the impact of the phenomenon on the surrounding population, the wind climate was analyzed. Then, improvement options were identified.

5. Analysis Climate of Wind in the Area of the Building

The time period in which the Carrasco weather station information is available, after elimination of "gaps" of data as well as the periods of time that this station does not operate, corresponds to a time series of velocity and

wind direction with duration equivalent to eight years. Based on the characteristics of the land surrounding the building and the weather station, a time series of hourly speed and wind direction data at the site of implantation of the building at the height of its roof was inferred.

As it is noted above, it is verified that for the generation of pure tones at frequencies of interest, due to vortex shedding from the holes in the perforated plate (**Table 3**), the occurrence of weather events with wind speed over 16 m/s is required at the level of the roof of the building (88 m high). The occurrence of weather events with wind speed greater than 16 m/s at 88 m on the site of implantation of the building under consideration was analyzed. Especially, we considered those winds with mean velocity exceeding 20 m/s. **Figure 7** shows that the wind roses for the study area are presented.

In **Figure 7(a)** the complete time series is considered while in **Figure 7(b)** only event with mean wind velocity of 20 m/s is included. The events considered would give rise to the events that could potentially lead to acoustic emissions in octave band of 4000 Hz. The data graphed in **Figure 7(b)** are presented in **Table 6**.

The total amount of these events would be around 0.96%, equivalent to about an average of seven monthly events. Higher probability of occurrence of these winds can be seen to winds from SOUTH and SOUTH-SOUTHWEST directions, meaning 54% of possible cases of interest.

It is assumed that the building of 120 m high, located towards SOUTHWEST-SOUTH-SOUTHWEST from the tower under study, protects it from the winds blowing from these directions, so the total number of events with the potential to cause discomfort will be 0.70%, which is equivalent to an average of 5 events per month or one per week.

If the shield was protected by installing a polycarbonate sheet, it would be possible to avoid the wind flow through their holes. If this protection was installed on the facades oriented towards the SOUTH and WEST, it would be possible prevent 96.3% of noise events.

The analysis of acoustic emissions generated by the interaction between the wind and the facade of a building has been presented. The occurrence of certain weather events generated noise emissions from such intensity perceived and might result in a potential cause of discomfort events interest.

From the theoretical developments presented and the results of field and wind tunnel measurements, we can infer that these acoustic emissions are generated by vortex shedding through the holes in the perforated plate installed due to flow winds exceeding speed of 20 m/s, at the height of the roof of the building (88 m high). These results are also associated with noise nuisance complaints made by the people who live and/or work in the study area.

Under these conditions, the characteristics of the sound spectra of the events of interest indicate a similar behavior, presenting strong pure tones in the octave band of 4000 Hz, which are perceived as a high-pitched sound

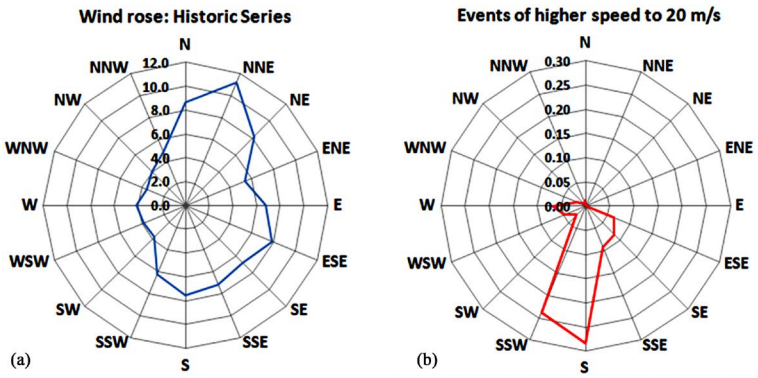

Figure 7. (a) Wind rose for relative frequencies of directions; (b) Wind rose to relative frequencies of direction and hourly average speeds above 20 m/s (both on the roof of the building).

Table 6. Percentage of time exceeding 20 m/s speed (also see **Figure 7 (b)**).

N	NNE	NE	ENE	E	ESE	SE	SSE	S	SSW	SW	WSW	W	WNW	NW	NNW
0.012	0.002	0.001	0.004	0.001	0.063	0.084	0.093	0.283	0.238	0.026	0.047	0.067	0.021	0.009	0.006

in the roof of the building and may cause feeling of annoyance because of their frequency and intensity to generate a similar perception of a broadband sound of (LA + 6) dBA [9], where LA is the sound pressure level of the broadband sound that has effectively occurred.

According to the analysis of winds for weather events that could potentially lead to event of annoyance associated to sound emissions, an average of 5 to 7 events per month would be registered. In order to mitigate these noise emissions, the installation of a polycarbonate shield on the existing metal shield on the facade of the building to avoid the wind flow through their holes could be proposed. If the shield is initially installed on the facades that are oriented towards SOUTH and WEST directions, the potentially annoying noise events would reduce 96.3%.

References

[1] Cataldo, J., Lisboa, M. and González, E. (2012) Análisis de emisiones acústicas en el edificio World Trade Center Free Zone. Facultad de Ingeniería, UdelaR. Montevideo, Uruguay.

[2] Simiu, E. and Scanlan, R.H. (1986) Wind Effects on Structures: An Introduction to Wind Engineering. John Wiley & Sons, Hoboken.

[3] Cataldo, J., *et al.* (2000) Programa de Evaluación de Calidad del Aire aplicado a la República Oriental del Uruguay. Informe Final, Convenio MVOTMA-UROU (Facultad de Ingeniería).

[4] Holmes, J. (2007) Wind Loading Structures. 2nd Edition, Taylor and Francis, UK.

[5] Blevins, R.D. (2003) Applied Fluid Dynamics Handbook. Krieger Pub Co., Malabar.

[6] Ahlborn, B., Seto, M. and Noack, B. (2002) On Drag, Strouhal Number and Vortex-Street Structure. *Fluid Dynamics Research*, **30**, 379-399. http://dx.doi.org/10.1016/S0169-5983(02)00062-X

[7] Abreu, J., Guarga, R. and Izquierdo, J. (1995) Oscilaciones hidráulicas en sistemas hidroeléctricos. Capítulo 14 en Transitorios y oscilaciones en sistemas hidráulicos a presión. Valencia, España.

[8] Crocker, M. (2007) Handbook of Noise and Vibration Control. John Wiley & Sons, Hoboken.

[9] ISO (2007) Acoustics. Description, Measurement and Assessment of Environmental Noise. Part 2: Determination of Environmental Noise Levels. ISO 1996-2:2007.

Open Journal of Acoustics, 2015, 5, 11-24
Published Online March 2015 in SciRes. http://www.scirp.org/journal/oja
http://dx.doi.org/10.4236/oja.2015.51002

Ultrasound Imaging in Nuclear Reactors Cooled by Liquid Metals

Victor D. Svet, Dmitrii A. Dement'ev

OJSC "N. N. Andreyev Acoustical Institute", Moscow, Russia
Email: vsvetd@mail.ru

Received 4 February 2015; accepted 6 March 2015; published 10 March 2015

Abstract

In nuclear reactors cooled by liquid metals, ultrasound is the only type of field that allows obtaining images of the reactor cores and diagnostics of the integrity of the fuel assemblies. The article discusses the features of the practical realization of ultrasonic imaging systems based on phased arrays and offers an alternative solution of imaging on the basis of the acoustic lenses of refractive and diffraction types. Using lenses eliminates many of the technical and technological problems associated with the development of multi-element phased arrays. It is shown that lens systems allow using traditional methods of transformation of acoustic fields into the visible images by 2D piezo matrix and a more promising way of acoustooptical transformation based on coherent optical interferometry.

Keywords

Ultrasound Imaging, Phased Arrays, Liquid Metals, Nuclear Reactors, Acoustic Lens

1. Introduction

Ultrasound imaging (UI) of objects located in molten metals is one of the most pressing problems of nondestructive testing in various industrial areas. Especially it is required in nuclear reactors cooled by liquid lead or sodium, as ultrasound is the only type of field to obtain images of objects disposed in the working zone of the reactor with a required high resolution. Researches in this area are carried out in different countries for decades [1]-[3], but to our knowledge, there is no commercial ultrasound imaging high-speed system capable to operate at temperatures up to 600˚C and high levels of radiation up to 30 kGy/h. The developed systems of ultrasonic imaging are based on the use of several transducers with their mechanical scanning in different planes. Such systems have low imaging speed and the mechanical scanning systems are quite complex [4]-[6]. In the overwhelming numbers of publications, multi-element phased arrays (MPA) are considering as the basis of UI [5]-[17]; so let's

How to cite this paper: Svet, V.D. and Dement'ev, D.A. (2015) Ultrasound Imaging in Nuclear Reactors Cooled by Liquid Metals. *Open Journal of Acoustics*, **5**, 11-24. http://dx.doi.org/10.4236/oja.2015.51002

consider the main problems which arise when developing phased arrays for ultrasound imaging in molten metals.

2. Ultrasound Imaging on the Base of Phased Arrays

Phased array is a distributed antenna system consisting of N individual receiving ultrasonic elements (piezoelectric transducers) arranged in a line (linear MPA) or in a two-dimensional matrix of $N*N$ elements. "Mill's Cross" configuration is often using, where one of the linear arrays is a receiver, and the second orthogonal linear array is a transmitter. Mill's cross arrays are widely used in ocean acoustic bathymetry, because instead of N^2 elements we can use only 2 N elements. It is well known that for high quality imaging receiving elements of array should have dimensions $\leq\lambda/2$, where λ—is a wavelength, and they should be regular. These are so called "full sampling arrays". Having this array it is possible to achieve the maximum viewing sector zone and minimum side field of array. In some applications the value of viewing sector can be reduced and array elements can have dimensions more that wave-length. But in this case the level of side field should be small to avoid unwanted artifacts in the ultrasonic images. The objects of interest in nuclear reactors are fuel rods and fuel assemblies. Their design and location determines the frequency band of ultrasound and hence the entire configuration of a further ultrasound imaging system. A typical image of the fuel element is shown in **Figure 1**.

The outer diameter of the fuel element is about 9 mm; the total length of fuel element with fastening elements is about 3840 mm. The fuel rods are usually collected in special cassettes (assemblies), a fragment of which is shown in **Figure 2**. Based on the above dimensions and requirements of NDT it is desirable to have a spatial resolution at least of 0.5 - 1 mm and less.

The most preferable mode is 3D ultrasound imaging. So the values of ultrasonic frequencies should be in the range 2···5 MHz. At sound velocity in the molten lead $C_l \approx 1750$ m/s, this corresponds to the wavelengths λ_{max} = 0.9 mm, λ_{min} = 0.35 mm. Therefore half-wave dimensions of elements should be from 0.45 mm to 0.18 mm and exactly these small dimensions create serious problems of design of phased arrays for ultrasound imaging in the liquid metals, although, for example, in the ultrasound systems for medicine or NDT such problems do not exist at all. Let's consider these problems in more detail.

2.1. Small Dimensions of Elements

Piezoelectric element with small dimensions has low capacity, <1 pF. Each element should be connected to a coaxial cable with length more than 15 meters. This is an average distance to signal processing system. Coaxial cables have specific capacity about 100 pF/m or more. This means that the level of the received signal will be reduced in thousands times, and it is necessary to take into account that nuclear power plants have very high levels of electromagnetic interference.

2.2. Low Sensitivity of Piezoelectric Ceramics

Despite the fact that the high-temperature piezoelectric ceramics exists, its sensitivity, defined by piezoelectric modulus d_{33} or d_{31} in several times less than that for low-temperature piezoelectric ceramics.

Figure 1. Fuel rod.

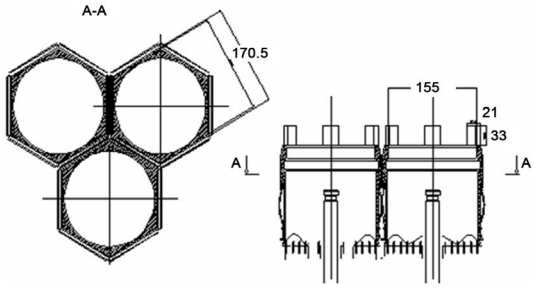

Figure 2. Fragment of fuel assembly.

2.3. Homogeneity of Array Elements

High-quality ultrasound imaging with phased arrays requires minimum level of the amplitude-phase spreading in the individual elements. Typical requirements are the following: sensitivity spread should be no more than ±3 dB, and phase spreads should not exceed ±5˚ at a higher frequency. For these requirements the array's directivity is close to calculated value.

2.4. Acoustical Cross-Talks

The gap between half wave elements in array for specified frequencies should be about 50 - 100 micrometers. In order to eliminate mutual influence of elements the gaps are filled with a special compound, the acoustic impedance of which should be in several times less than acoustic impedance of the piezoelectric element. For low temperatures such compounds are well known. For specified conditions only high-temperature compounds such as epoxy resins can be used and their acoustic impedance is close to the impedance of elements and required decoupling of elements is problematic. According to some published data level of decoupling is (−10 - 12 dB), which is clearly not enough [8]-[10].

2.5. Temporary Temperature Instability

At high temperatures, the various parameters of PZT are very sensitive to temperature fluctuations (especially value of piezomodules, resonance frequency, etc.) which lead to strong amplitude and phase fluctuations in the received signals.

2.6. Wettability.

Most of the liquid metals have poor wettability, which decrease acoustic contact of array's elements with the working environment. In particular, lead has poorer wettability. In order to improve the wettability many authors proposed coating of array's elements with different metal films-gold, nickel and other [9] [10].

In connection with these problems "half-hearted" solutions are suggested in many publications. First of all, the dimensions of elements in arrays are chosen much larger than the half wavelength [10] [12]. This reduces the value of viewing sector which is determined as

$$\theta^0 = \pm 50\frac{\lambda}{d} \quad (\text{on} - 3\text{dB level}) \tag{1}$$

where λ—wavelength of the ultrasound, and d—the dimension of the element. According [14] the dimension of one element in matrix array on 36*36 elements at a frequency 5 MHz, had a size of 2.5 × 2.5 mm, and furthermore, elements were located within 5 mm gap from each other. Array was designed for operation at 200˚C. Therefore view angle of this array should not exceed ±10˚, and moreover because of not full sampling 100% side lobes must appear in array directivity patterns. To provide wide view sector such matrix array had to be mechanically rotated, that virtually "negates" all the advantages of phased arrays. Realizing that a large number of elements in the matrix array create serious technological problems, many authors have "returned" to the development of so- called "randomized" arrays, *i.e.* arrays with a random arrangement of receiving elements [18]. This old idea, borrowed from radar of 1960th years has well recommended itself in applications for focused ultrasound surgery where it is necessary to create one focal point. However, in our opinion, randomization of arrays is a not good solution because of unpredictable occurrence of additional peaks in directivity patterns and unpredictable level of the side field. Mill's cross arrays [19] [20], can provide imaging in a wider viewing sector but they require consistent changing of the vertical beam angle of the transmitting array. Using simultaneous transmission of orthogonal signals in several vertical directions , reduces the output signal/noise ratio, since for any radiated signal at a predetermined vertical angle, all other transmitted orthogonal signals are noise, and, in addition, such a system is quite complex.

This brief review shows that for high quality ultrasound imaging, especially in 3D mode, the dimensions of the receiving elements must be no more half-wavelength and wavelength. And assuming that the connection technology (splicing) of small size elements with coaxial cables is worked out, the compensation of signal losses must be done by preamplifiers in array housing. This design will inevitably require forced cooling.

3. Ultrasonic Lens Imaging

Many of discussed problems can be eliminated if we will use acoustic lenses for imaging instead of phased arrays. Such lens systems are widely used in underwater acoustic imaging and sonar [21]-[23]. The main advantage of this solution is that the acoustic lens automatically forms image in some plane and it can be simply registered. In continuous mode acoustic image is constructed only in the transverse coordinates, and the problem of phasing of individual array elements is automatically eliminated, as only the intensity of image can be registered. Moreover, acoustic lens allows offering a variety of ways of transforming acoustic image into a visible image, which will be discussed later. The disadvantage of lens systems is a rather small view angle. For a single lens, its value is no more than 26˚ - 30˚, but may be extended up to 45˚ - 50˚ by using more complex acoustic lens objective. For operation in the liquid lead or liquid sodium the acoustic lens may be made from metal (steel, titanium, tungsten). Wave size of lens should conform to the required angular resolution at a given frequency. **Figure 3** shows the possible arrangements of lens imaging systems. The acoustic lens can be formed as the refractive focusing elements or diffractive lenses.

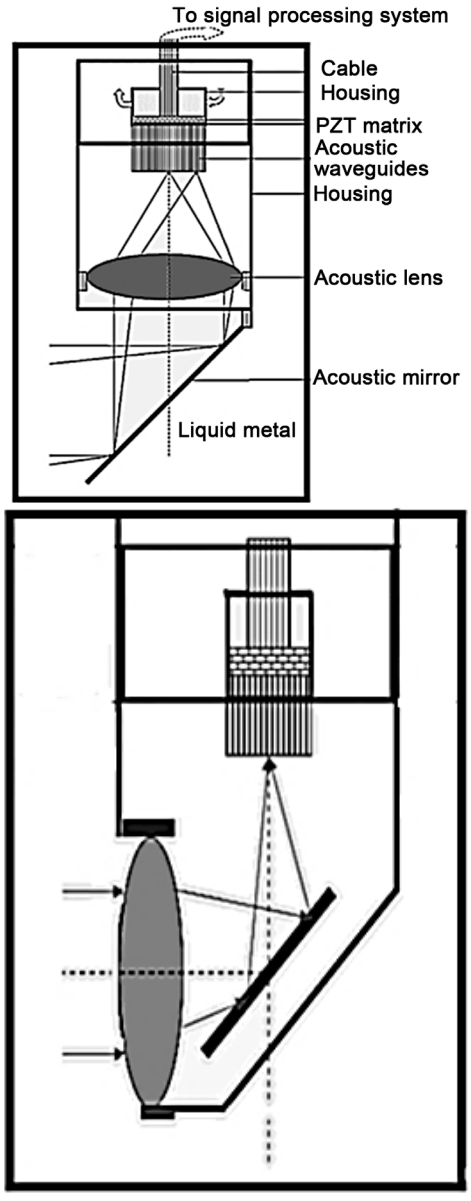

Figure 3. Variants of arrangements of acoustic lens.

3.1. Refractive Acoustic Lenses

Refractive acoustic lens are similar to a conventional optical lens; the only difference is that depending on the sound speed in the material of the lens and in the environment, the forms of lens can be converging and diverging. The quality of the acoustic image is largely dependent on the parameters of the acoustic lens and its form. It was found that the optimal form of a single lens is convex-concave lens, which has sufficient view angle and a relatively low level of side lobes (without apodization), [23], **Figure 4**.

Calculations and experiments have shown that this single simple lens capable to build undistorted image with the given parameters and angular resolution in view sector no more than ±15˚. In the sector of angles ±22.5˚ due to aberrations angular resolution worsens in 1.5 times. So at a frequency of 3.5 MHz in the view sector ±12.5˚ transverse resolution is 0.8 mm, and for view sector ±22.5˚ it increases to 1.3 mm. **Figures 5(a)-(c)** show a longitudinal section of the acoustic field for angles −20˚, 0˚, 20˚ (**Figure 5(a)**) and forms of the focal spots at normal incidence (**Figure 5(b)**) and at an angle of −10˚ (**Figure 5(c)**).

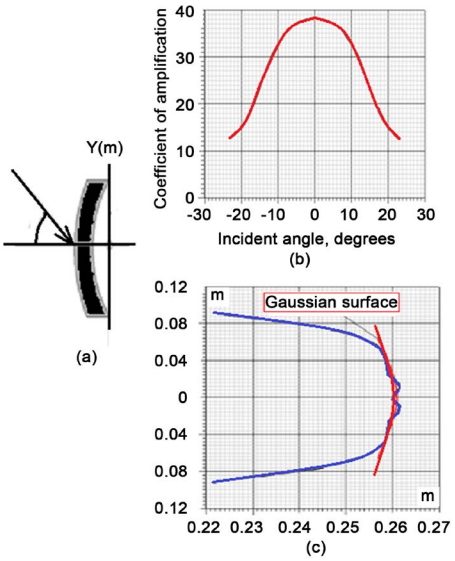

Figure 4. Calculated parameters of acoustical lens from steel for frequency F = 3.5 MHz and diameter 120 mm. (a) Form of lens; (b) Coefficient of amplification; (c) The form of focal surface in longitudinal section.

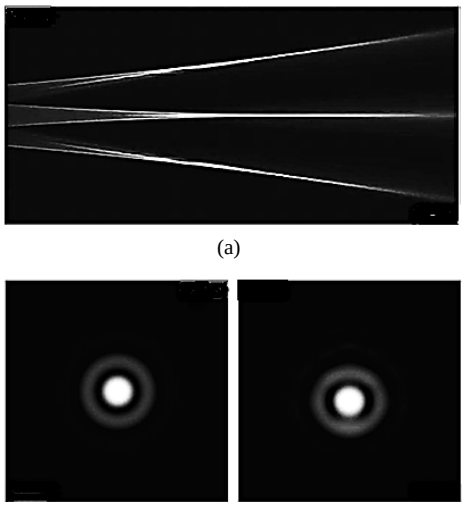

(a)

(b) (c)

Figure 5. Images of longitudinal sections (a); and focal spots (b).

Figure 6(a) shows images of longitudinal sections of 10 of point sources, and. their amplitude distribution in a lateral section (**Figure 6(b)**).

Photos of acoustic lens made from steel with a diameter of 90 mm and 120 mm for frequencies 3.5 and 1.5 MHz accordingly are presented on **Figure 7**.

3.2. Diffraction Acoustic Lenses

In acoustics diffraction lenses are known as the "zone plates" or Fresnel lenses. The rapid development of digital optics stimulated again big interest to diffraction lens due to possibility to eliminate the associated diffraction beams and significantly increasing the diffraction efficiency. The basic idea of such a binary structure is that the phase of the diffracted beam may be encoded by different heights of zone rings. In this case, the diffraction efficiency of a coded zone plate is

$$\eta = \left[\frac{\mathrm{Sin}(n/N)}{n/N}\right]^2 \tag{2}$$

where N-number of equal levels of phase encoding. For example, eight coding levels provide 95% diffraction-

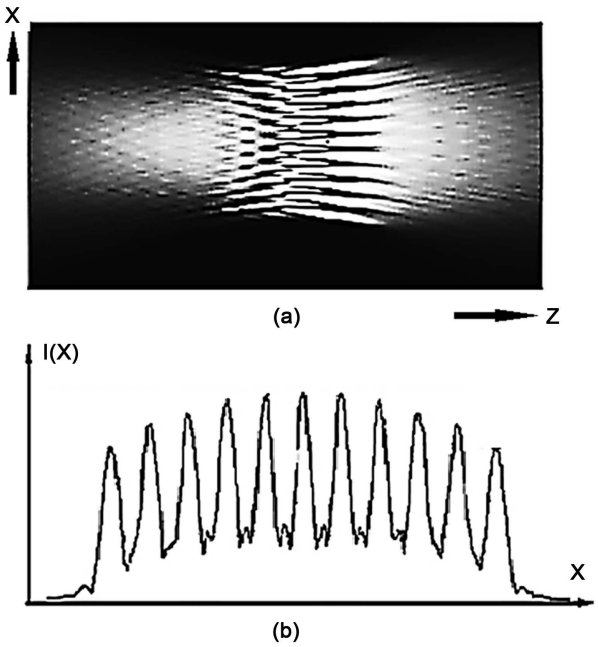

Figure 6. Images of focused 10 points in longitudinal (a) and lateral (b) sections.

Figure 7. Prototypes of steel acoustical lenses for frequencies F = 3.5 MHz (left image) and F = 1.5 MHz (right image).

efficiency of zone lens, while conventional refractive lenses have diffraction efficiency of at least 75%. For each level of the coding phase the local ring radius is calculated by the formula

$$r_\kappa = \left[\left(z_0 + k\frac{\lambda}{N}\right)^2 - z_0^2\right]^{0.5} \tag{3}$$

where z_0—focal length, λ—wavelength, and the sampling interval is defined as

$$\Delta = \frac{1}{Nf\left(\frac{1}{C_m} - \frac{1}{C_l}\right)} \tag{4}$$

where f—frequency, C_m, C_l—sound velocities in the environment and the material of the lens, respectively. Scheme of the diffraction zone lens with 4 coding levels is presented in **Figure 8**.

Note that for ultrasound imaging in lead binary diffraction lens is of great interest. First of all, its weight is significantly less than weight of refractive lens, and it is much easier for manufacturing. Given the high level of radiation a working zone, lens can be manufactured from a wide range of materials which do not have an increased resistance to radiation, and a lens can be replaced quickly. Moreover, the zone lens has small parasitic reflections from their surfaces in comparison with refractive lens. The only drawback is that diffraction lens has rather narrow frequency band, *i.e.* such focusing systems have elevated "chromatic" aberration, but this question requires special consideration.

4. Registration of the Signals in the Lens System by PZT Matrix

Let us now consider how to register acoustic image. One of the solutions is based on the use of two-dimensional PZT matrix made of low-temperature ceramics with a big value of the piezoelectric modulus d_{33}. Acoustic coupling of matrix with the liquid metal can be carried out through matrix solid waveguides with a diameter smaller than the ultrasonic wavelength [24]. PZT matrix itself can be located in a small hermetic cooling case, **Figure 9(a)**. Outer ends of the acoustic waveguides can be positioned on a curved surface (Gaussian plane) to minimize the aberration of the lens. The form of this shape is calculated in advance. Decoupling of acoustic waveguides is achieved by their placement in a porous high-temperature ceramics, which acoustic impedance is

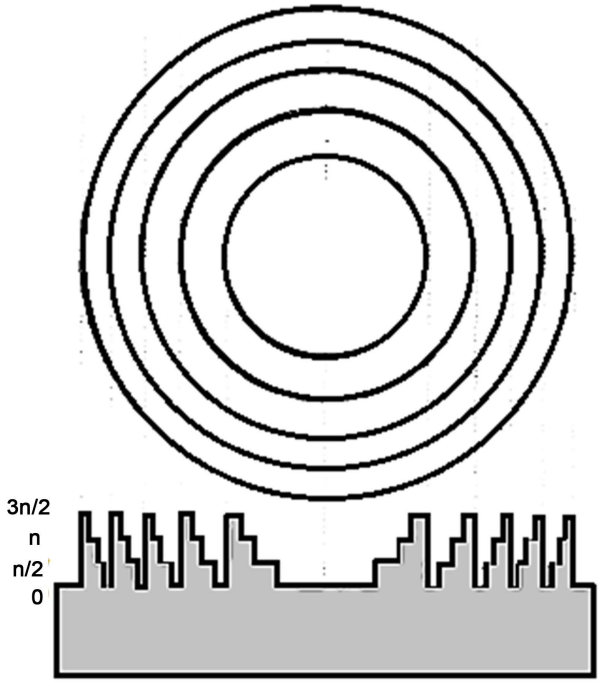

Figure 8. Zone binary lens with 4 encoding levels.

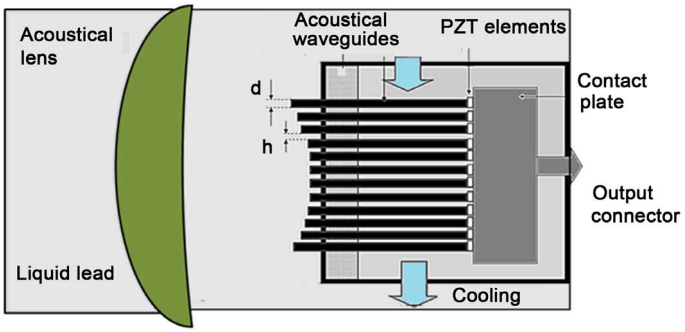

(a)

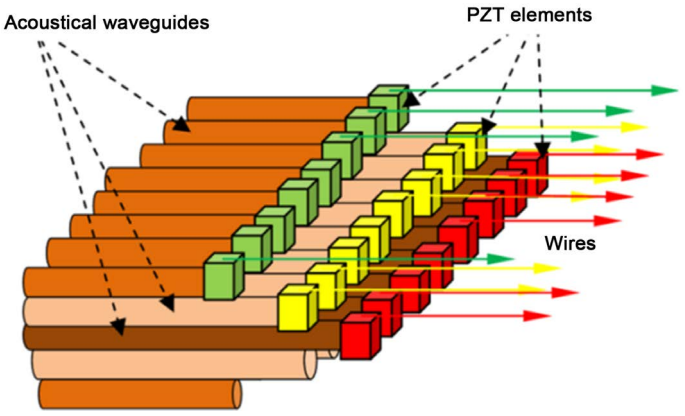

(b)

Figure 9. (a) Lens imaging system with 2D PZT matrix; (b) Wiring of PZT elements.

much smaller than acoustic impedance of the acoustic waveguide. Porous carbon structures and high temperature silicon resins are also promising materials. The use of different lengths of the acoustic waveguide which output ends are connected with PZT elements allows diluting the connecting wires in space, **Figure 9(b)**. Note also that adding a second lens we can increase the size of the output acoustical image, and increase the dimensions of PZT elements *i.e.* increase their capacity and weaken the requirements to the next electronics.

Sensitivity of reading system depends on the length of acoustic waveguides and the parameters of the materials from which they are made. If the diameter of the waveguide is less than wavelength the equation for propagation of longitudinal waves is

$$\frac{\partial^2 \xi}{\partial t^2} = \frac{E}{\rho}\frac{\partial^2 \xi}{\partial X^2} + \frac{E'}{\rho}\frac{\partial^3 \xi}{\partial t \partial X^2} \tag{5}$$

Boundary conditions are as follows. In the section at $X = 0$, where the external pressure is applied there is a tension generated by this pressure P:

$$\left(E + i\omega E'\right)\frac{\partial \xi(X)}{\partial X} = P \tag{6a}$$

The second end of the rod at $X = l$ is free and therefore the tension is zero:

$$\left(E + i\omega E'\right)\frac{\partial \xi(X)}{\partial X} = 0 \tag{6b}$$

The solution of equation with these boundary conditions is given by [24]:

$$\xi(X,t) = -\frac{P\exp(i\omega t)ch\left[ik'(l-X)\right]}{ik'\left(E + i\omega E'\right)sh(ik'l)} \tag{7}$$

where E and k are related by

$$\kappa = k + ik' = \frac{2\pi}{\lambda} + i\alpha = \omega\sqrt{\frac{\rho}{E + i\omega E'}}$$

For a rod with small damping when $\omega E' < E$, the formula for $X = l$ can be rewritten as:

$$\xi(l,t) = -\frac{P \cdot \exp(i\omega t)\left\{\cos\left[\frac{\omega}{C_{\text{CT.}}}(l-x)\right] + i\delta(l-x)\sin\left[\frac{\omega}{C_{\text{CT.}}}(l-x)\right]\right\}}{i \cdot k'(E + i\omega E')\left[i \cdot \sin\left(\frac{\omega l}{C_{\text{CT.}}}\right) + \delta \cdot l \cdot \cos\left(\frac{\omega l}{C_{\text{CT.}}}\right)\right]}. \quad (8)$$

Figure 10 shows the calculated values according to the displacement end of the rod depending on its length at different frequencies at the following initial parameters: the medium-liquid lead, a density of 10.9×10^3 kg/m^3, the velocity—1750 m/sec. Waveguide has the length l with diameter d, made from steel with a density ρ_2 = 2320 kg/m^3 and the sound speed C_2 = 5500 m/s. The amplitude of the pressure in lead is P = 1 Pa. The amplitude of the pressure in the rod is equal to P = 0.8 Pa.

Note that ultrasonic imaging lens system allows the use of pulse mode for 3D imaging. However, as waveguides have different lengths it is necessary to compensate small time delays, which can be implemented in signal processing unit.

5. Acoustooptical Registration of Image

The use of acoustic waveguides allows offering an alternative conversion of acoustical image into visible image by direct acoustooptical transformation, for example by laser vibrometer, **Figure 11**.

The principle of the laser vibrometer is based on measuring the Doppler frequency shift of light reflected from a moving object. For such measurements optical heterodyne method is commonly used on the basis of a two-beam interferometric optical scheme with the subsequent formation of the quadrature components of the electrical signal and photo detectors of the balanced type. Modern methods of laser vibrometry have a very high sensitivity and resolution in the frequency range of vibrations up to hundreds of MHz's. For example, a laser vibrometer PSV-500M POLYTEC allows scanning vibrating surface from distances 0.1 m up to 100 meters in the field of view of 50˚*40˚ with angular resolution 0.002˚. Minimum detectable displacement is 10^{-12} m. The scanning speed is several hundred points/sec. Such high angular resolution allows setting the laser vibrometer at height, for example, 10 meters from the vibrating ends of the waveguides and scanning area will be only 0.35 mm^2.

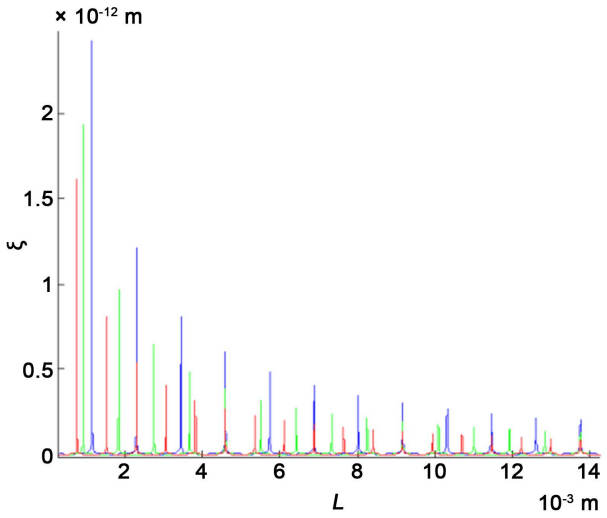

Figure 10. Calculated values of displacements (m) versus length of waveguide (m) for different frequencies. Red—3.6 MHz, Green—3 MHz, Blue—2.5 MHz.

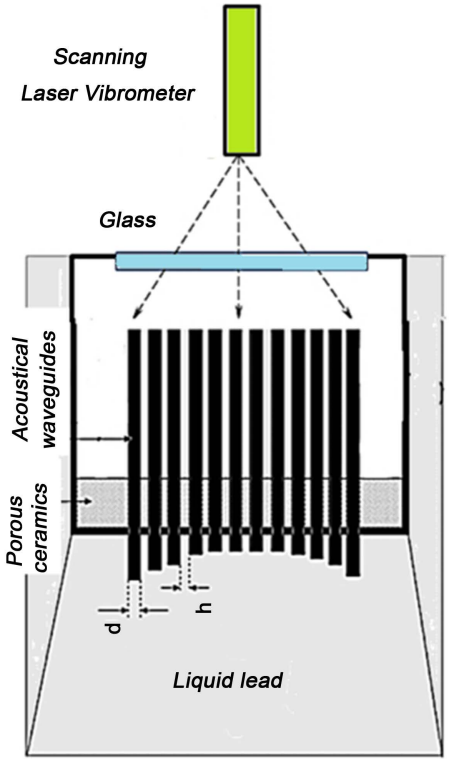

Figure 11. Reading of acoustical image by laser vibrometer.

It is possible to use other scheme of optical reading, also based on the interferometric optical system, but without a scanning laser [25]. The idea of this scheme is as follows. At a distance d from the output ends of waveguides the plane-convex lens is placing. Plane flat surface of this lens and the plane of the output end form a multichannel Fabry-Perot interferometer. Using a laser and a collimator formed by a plane-convex lens and other lens parallel light beam is forming which illuminates the ends of the waveguides. The reflecting light from the ends is forming an interferometry pattern, which intensity $I(x, t)$ is modulated by the incident acoustic field $P(x, t)$. Modulated distribution $I(x, t)$, via the lens system is projected on the photo-detector matrix, like CCD camera and then enters a signal processing device, where optical image is forming. The distance d between the output ends of the acoustic waveguide and plane-convex lens is as follows:

$$d = d_0 + \xi \mathrm{Cos}\left(\omega_{ac} t\right)$$

where ξ—vibrational displacement of the output end of the acoustic waveguide, ω_{ac}—circular frequency of the ultrasound, and the gap d_0 is chosen from the condition of quadrature detection:

$$d_0 = \frac{n\lambda}{4} + \frac{\lambda}{8} \tag{9}$$

where n—integer and λ—wavelength of light.

The output light intensity of such an interferometer is

$$I = \left(I_1 + I_2\right)\left[1 + \chi \mathrm{Cos}\varphi\right] \tag{10}$$

where I_1 and I_2—the intensity of the light waves reflected from the ends of the waveguides and the flat surface of the lens,

$$\chi = 2\left(I_1 I_2\right)^{1/2} \Big/ \left(I_1 + I_2\right)$$

$$\varphi = \frac{4\pi}{\lambda} d = \pi n + \frac{\pi}{2} + 4\pi \frac{\xi}{\lambda} \mathrm{Cos}\left(\omega_{ac} t\right) \tag{11}.$$

Thus the output light intensity is equal to

$$I = I_0\left[1+\chi \mathrm{Sin}\left(4\pi\frac{\xi}{\lambda}\mathrm{Cos}\left(\omega_{ac}t\right)\right)\right] \tag{12}$$

And when $\xi \ll \lambda$ expression (12) takes the form

$$I \approx I_0\left[1+4\pi\chi\frac{\xi}{\lambda}\mathrm{Cos}\left(\omega_{ac}t\right)\right] \tag{13}$$

i.e., the output optical signal is proportional to the amplitude of the oscillatory displacement (or sound pressure) of the local acoustic waveguide at the working point $\left(I_{\max}+I_{\min}\right)/2$, **Figure 12**.

Figure 13 shows a possible scheme implementing the method discussed above.

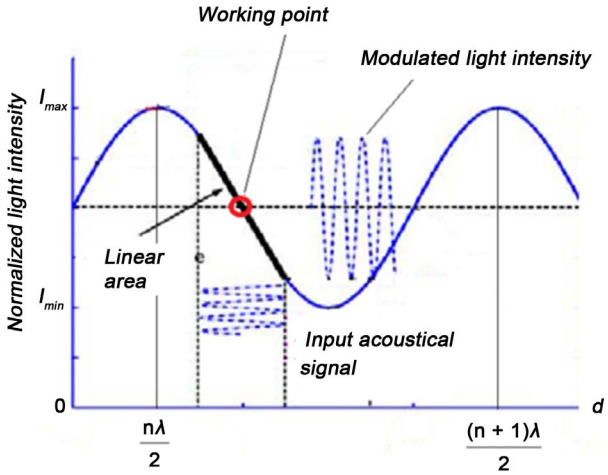

Figure 12. Selection of working point.

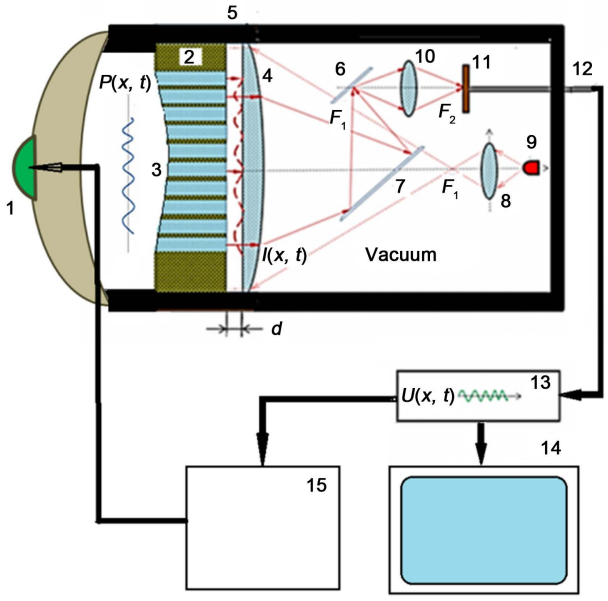

Figure 13. Optical reading scheme on the base of interferometer Fabry-Perot. 1. Acoustical lens with transducer; 2. Porous ceramics; 3. Waveguides; 4. Plane-concave lens; 5. Housing; 6, 7. Optical mirrors; 8, 10. Spherical lens; 9. Semiconductor laser; 11. CCD matrix; 12. USB cable; 13. Signal processing unit; 14. Display; 15. Signal generator.

System elements (4-11) are arranged in the housing, from which air is evacuated in order to avoid parasitic effects of refraction of the optical waves in a high temperature environment. The distance d between the output ends of the waveguides and the planar surface of lens diameters and output ends of the waveguides is chosen so that the diffraction divergence of the light from each end of the waveguide is small and reflected light from the output ends do not overlap that minimizes interference of the reflected optical signals. In the presence of field $\xi(x, t)$ spatial distribution of the interference pattern arises and the spatial distribution of the light intensity $I(x, t)$is proportional to $\xi(x, t) \sim P(x, t)$. Using optical mirrors (6, 7) and the objective (10) the spatial distribution $I(x, t)$ is projected onto the CCD matrix (11), connected with the signal processing device (13). Projecting an image is performed by a double Fourier transformation implemented by a plane-convex lens (4) and the lens (10), having equal focal lengths.

Non-contact optical method for reading the acoustic image has many advantages compared with traditional methods of piezoelectric conversion. First of all, there is no piezoelectric matrix itself and, consequently, all problems related to cooling, distributing large number cables and connections are eliminated. Moreover, high-energy power systems are characterized by high electrical and electromagnetic interference and optical reading is not sensitive to this noise.

6. The Acoustic Transmitter

Source level of ultrasonic transmitter must be sufficiently high. Other important requirement is the uniformity of illumination of the working area. Fortunately, at higher frequencies, generation high levels of acoustic pressure do not constitute a serious problem. For a lens system (no matter of what type), it is conveniently to place transducer n the center of lens because it is practically not "working" for imaging. Another variant is to place transducers around the lens. Below several variants of transmitters and their calculated distribution of the pressure field are presented. Since the frequencies are in the range from 1.5 to 3.5 MHz, the increasing diameter of the radiator to several wavelengths increases its directivity (1). If the dimension of transmitter is about 1 mm or slightly more for the frequency F = 3.5 MHz, it will have the desired directivity about 45˚, but the intensity of radiation will be extremely low, since nigh voltages will destroy such small element. It follows that the transmitter must consist of groups of PZT elements of suitable dimensions. There are several variants of this design. One of the simulated versions is shown in **Figure 14(a)**.

It is a hemisphere covered by elementary transducers or solid hemisphere with a predetermined diameter and radius of curvature. The second embodiment of the transducer is shown in **Figure 14(b)**, and it represents a group of radiating elements disposed along the perimeter of the lens. The signals of all elementary transducers in both versions are transmitting in phase. Below there are some examples of calculated acoustics fields. The first transducer had a diameter 6 cm and a radius of curvature of 10 cm, maximum intensity on the element is approximately 2 W/cm^2. We see that from a distance 30 cm, the radiated field has good uniformity and a sufficient view angle. Blue color on **Figure 15(a)** corresponds to acoustical pressure more than 10^5 Pa on F = 3 MHz. **Figure 15(b)** shows the distribution of pressure for the ring transducer consisting of 20 elements with a diameter of 1 cm. This transducer has the same acoustic pressure of 10^5 Pa with the field in homogeneity about ±3 dB.

7. Conclusion

The discussed peculiarities of ultrasonic imaging in molten metals permit to conclude that lens imaging system

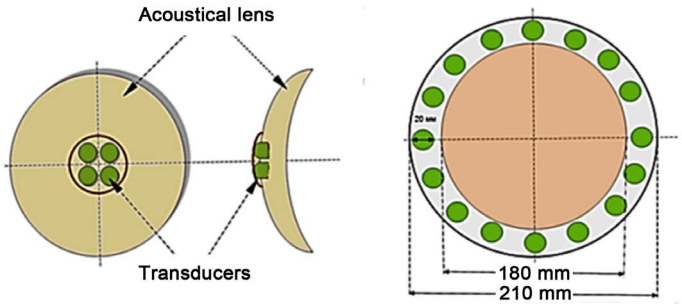

Figure 14. Variants of combined acoustical transmitters (a) in the center of lens (b) ring set of transducers.

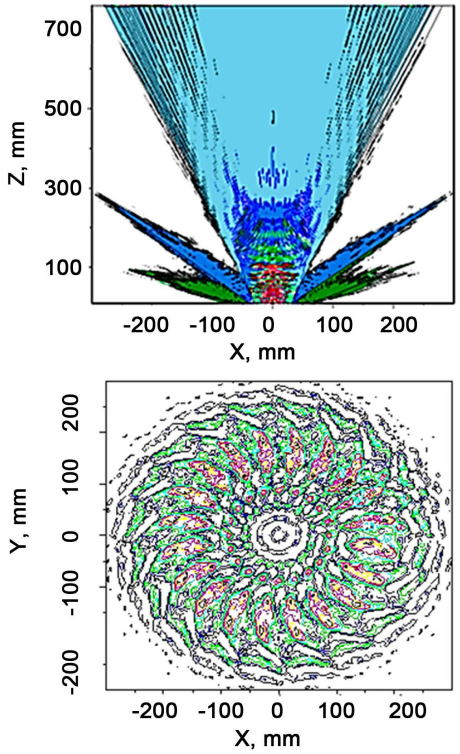

Figure 15. Beam patterns of transducers (**Figure 14(a)** and **Figure 14(b)**).

compared with phased arrays has many serious advantages and can eliminate many technological and design problems associated with the development of multi-element phased arrays. Lens systems allow realizing as traditional methods of reading signals by 2D PZT matrix and optical interferential methods of transformation of acoustical image into optical one. This variant in our opinion is the most promising technical solution for the development of ultrasonic imaging systems for nuclear reactors' cooling by liquid metals.

Acknowledgements

The authors thank S. Baykov, L. Gavrilov and S. Petrosyan for help in performing the simulations and K. Mikheev for valuable advices and consultations. The authors are also grateful to the participants of seminar of Prof. S. A. Ribak "Acoustics of inhomogeneous media" for a fruitful discussion of this work.

This work is supported by GRANT RFBR 14-02-00331.

References

[1] Barrett, L.M., McKnight, J.A. and Forthergill, J.R. (1984) Ultrasonic Viewing in Fast Reactors. *Physics in Technology*, **15**, 308-314. http://dx.doi.org/10.1088/0305-4624/15/6/I03

[2] Griffin, J.W., *et al.* (2009) Under Sodium Viewing: A Review of Ultrasonic Imaging Technology for Liquid Metal Fast Reactors. Pacific Northwest National Laboratory, Richland, PNNL-18292.

[3] Jasiūnienė, E. (2007) Ultrasonic Imaging Techniques for Non-Destructive Testing of Nuclear Reactors, Cooled by Liquid Metals, Review. *Ultragarsas* (*Ultrasound*), **62**.

[4] Takagi, K., Otaka, M., Arai, T., Yoda, S., Nagai, S., Suzuki, T., Miura, T. and Karasawa, H. (2000) Development of Novel Visualization Technique of Flow Field for Liquid Metals Using High Temperature Ultrasonic Transducer. *Proceedings of the* 2000 *ASME Fluids Engineering Division Summer Meeting*, Boston, 11-15 June 2000, 331-336.

[5] Kazys, R., Voleisis, A., Sliteris, R., Mazeika, L., Van Nieuwenhove, R., Kupschus, P. and Abderrahim, H.A. (2002) Investigation of Ultrasonic Properties of a Liquid Metal Used as a Coolant in Accelerator Driven Reactors. 2002 *IEEE Ultrasonics Symposium*, **1**, 815-818.

[6] Bond, L.J., Doctor, S.R., Bunch, K.J., Good, M.S. and Waltar, A.E. (2007) Instrumentation, Monitoring and NDE for New Fast Reactors. *Advanced Nuclear Fuel Cycles and Systems* (*GLOBAL* 2007), Boise, 1274-1279.

[7] Griffin, J.W., Bond, L.J., Jones, A.M. and Peters, T.J. (2010) Design of High Temperature Ultrasonic Linear Arrays for Under-Sodium Viewing. 7*th International Topical Meeting on Nuclear Plant Instrumentation, Control and Human Machine Interface Technologies* (*NPIC&HMIT* 2010), Las Vegas, 7-11 November 2010, 1600-1614.

[8] Abderrahim, H.A., *et al.* (2003) MYRRHA, a Multi-Purpose Accelerator Driven System for R&D. State-of-the-Art of the Project at Mid-2003. *Proceedings of International Workshop on P&T and ADS Development*, Mol, Belgium, 6-8 October 2003.

[9] Kažys, R., Voleišis, A., Šliteris, R., Voleišienė, B., Mažeika, L., Kupschus, P. and Abderrahim, H.A. (2006) Development of Ultrasonic Sensors for Operation in a Heavy Liquid Metal. *IEEE Sensors Journal*, **6**, 1134-1143. http://dx.doi.org/10.1109/JSEN.2006.877997

[10] Kažys, R., Voleišis, A., Šliteris, R., Mažeika, L., Van Nieuwenhove, R., Kupschus, P. and Abderrahim, H.A. (2005) High Temperature Ultrasonic Transducers for Imaging and Measurements in a Liquid Pb/Bi Eutectic Alloy. *IEEE Transactions on Ultrasonics, Ferroelectrics, and Frequency Control*, **52**, 525-537. http://dx.doi.org/10.1109/TUFFC.2005.1428033

[11] Kažys, R., Mažeika, L., Jasiūnienė, E., Šliteris, R., Kupschus, P., Van Nieuwenhove, R. and Abderrahim, H.A. (2003) Ultrasonic Imaging Techniques for the Visualization in Hot Metals. *Proceedings of the World Congress on Ultrasonics*, Paris, 7-10 September 2003, 1391-1394.

[12] Kažys, R., Mažeika, L., Voleišis, A., Šliteris, R., Jasiūnienė, E., Abderrahim, H.A. and Dierckx, M. (2007) Ultrasonic Imaging in the Liquid Metals. *International Journal of Applied Electromagnetics and Mechanics*, **25**, 249-256.

[13] Rajendran, A., Asokane, C., Elumalai, G. and Swaminathan, K. (1996) Development of an Ultrasonic Under-Sodium Scanner for the Fast Breeder Test Reactor. *Proceedings of the* 14*th World Conference on Non-Destructive Testing*, New Delhi, 8-13 December 1996, 349-352.

[14] Karasawa, H., Izumi, M., Suzuki, T., Nagai, S., Tamura, M. and Fujimori, S. (2000) Development of Under-Sodium Three-Dimensional Visual Inspection Technique Using Matrix Arrayed Ultrasonic Transducer. *Journal of Nuclear Science and Technology*, **37**, 769-779. http://dx.doi.org/10.1080/18811248.2000.9714955

[15] Swaminathan, K., Rajendran, A. and Elumalai, G. (1990) The Development and Deployment of an Ultrasonic Under-Sodium Viewing System in the Fast Breeder Test Reactor. *IEEE Transactions on Nuclear Science*, **37**, 1571-1577.

[16] Imbert, C., Berton, J.L. and Gimenez, N. (1996) Realization of Ultrasonic Images of Immersed Metallic Structures Using a Digital Beam Forming System. Experimental Study. *Proceedings of the* 1996 *IEEE Ultrasonics Symposium*, San Antonio, 3-6 November 1996, 765-770.

[17] Song, S.-J., Shin, H.J. and Jang, Y.H. (2002) Development of an Ultra Sonic Phased Array System for Nondestructive Tests of Nuclear Power Plant Components. *Nuclear Engineering and Design*, **214**, 151-161.

[18] Yang, P., Chen, B. and Shi, K.-R. (2006) A Novel Method to Design Sparse Linear Arrays for Ultrasonic Phased Array. *Ultrasonics*, **44**, 717-721. http://dx.doi.org/10.1016/j.ultras.2006.05.131

[19] Martin, L., Pepe, D. and Dupraz, R. (2002) Lifetime Extension of the Phenix Nuclear Power Plant. *Proceedings of a Technical Meeting*, Cadarache, 11-15 March 2002, 83-91.

[20] Giraud, M., Major, P., Gros, J., Martin, L., Benoist, P. and Burat, O. (2002) Advanced and Innovative Approaches to Inspect the Phenix Fast Breeder Reactor. *Proceedings of a Technical Meeting*, Cadarache, 11-15 March 2002, 83-98.

[21] Belcher, E.O. (1999) Limpet Mine Imaging Sonar. *Proceedings of the* 13*th Annual International Symposium on Areo Sense*, Orlando, April 1999, 2-10.

[22] Belcher, E.O., Lynn, D.C., Dinh, H.Q. and Laughlin, T.J. (1999) Beamforming and Imaging with Acoustic Lenses in Small, High-Frequency Sonars. *Proceedings of Oceans* 99*MTS\IEEE*, Seattle, 13-16 September 1999, 1495-1499.

[23] Baikov, S.V., Svet, V.D. and Sizov, V.I. (2000) Experimental Investigation of the Resolution and Sensitivity of Ultrasonic Imaging Camera with an Immersion Lens. *Akusticheskij Zhurnal*, **46**, 596-600.

[24] Korobov, A.I., Burov, V.A., Dmitriev, K.V. and Rumyantseva, O.D. (2012) Resonance Acoustical Spectrometry of Solids. Physical Department, Moscow State University, Moscow, 30.

[25] Svet, V.D., Dement'ev, D.A. and Galoutin, V.Z. (2014) On Some Problems of Ultrasonic Visualization of Objects in Liquid Metals. *Proceedings of the First Russian Acoustical Conference*, Moscow, 6-10 October 2014.

Open Journal of Acoustics, 2015, 5, 25-28
Published Online March 2015 in SciRes. http://www.scirp.org/journal/oja
http://dx.doi.org/10.4236/oja.2015.51003

The Failure of the Cross Correlation Measurement Technique

Ken McGill, Kathryn Harke, Kris Schock

Department of Chemistry, Physics, and Astronomy, Georgia College and State University, Milledgeville, GA, USA
Email: ken.mcgill@gcsu.edu

Received 17 February 2015; accepted 7 March 2015; published 10 March 2015

Abstract

The experiment involves creating a sound wave that propagates down a pipe with 8 transducers attached at equally spaced intervals of 0.01016 m. The numerical method—the Cross Correlation Method, used to solve for the phase component, creates a high correlation value, but the speed of sound varies immensely. The method involves a Fast Fourier Transform (FFT) of the collected data, which is used to find the phase of the sound wave, and the slope of the position versus time graph, which is used to calculate the speed of sound. This high correlation value shows that the data are correct, but the numerical method for analyzing the data is incorrect.

Keywords

Acoustic Array, Cross Correlation, Flow Measurement

1. Introduction

Since the establishment of the first oil transporting pipeline system in 1879, half a million miles of pipe line networks have been built across the United States [1]. With the rising nationwide demand for various commodities such as water, petroleum, and natural gas, the expansion of the pipeline system was a necessity as a means of transportation for millions of dollars of valuable merchandise. With the growing number of pipelines nationwide and the increasing volume of liquids transported daily via pipeline, a newfound need has arisen for technology that accurately calculates the rate of flow of these liquids. In order to control the amount of a substance sent through a pipe, the measure of its flow velocity must be determined to a high level of accuracy. Various techniques and technologies have been created in an attempt to provide an accurate measurement for flow in a closed conduit; however, they offer results with varying degrees of inaccuracies. The Cross Correlation Method has become a popular method in determining rate of flow through a pipeline [2]. A proposed acoustic method

How to cite this paper: McGill, K., Harke, K. and Schock, K. (2015) The Failure of the Cross Correlation Measurement Technique. *Open Journal of Acoustics*, **5**, 25-28. http://dx.doi.org/10.4236/oja.2015.51003

employs a set of transducers along the measured pipe which detect time delay for an acoustic wave propagating through the pipe.

2. Theory

The Wave Equation

A solution to the wave equation for a sound wave propagating through a pipe is:

$$\Psi = A\sin\left(k\left(x+\pi\sin\right)\right) = \pi A\sin\left(\frac{2\pi}{\lambda}\left(x+\lambda ft\right)\right) = A\sin\left(2\left(\frac{x}{\lambda}+ft\right)\right) = A\quad\left(\theta+\quad ft\right) \tag{1}$$

where A is the normalization constant, k is $(2\pi)/\lambda$, f is the frequency of the wave, t is the time, x is the position, λ is the wavelength of the wave, and θ is the phase angle of the wave propagating through space [3]. By comparing the arguments of the functions sin ( ) in equality (1), one can see that the phase plotted versus the position will include the speed of sound [3].

$$\theta = 2\pi\frac{x}{\lambda} = \frac{fx}{c} \tag{2}$$

$$m = \frac{2\pi f}{c} \tag{3}$$

where m is the slope of the line. Thus, the speed of sound, c, can be found as follows:

$$c = \frac{2\pi f}{m} \tag{4}$$

3. Procedure

In an experiment to test this proposed method, 450 distinct frequencies of sound waves from 500 to 5000 Hz were sent down a 7.50 m long metal pipe with a 0.1524 m diameter **Figure 1**. The range of 500 to 5000 Hz was chosen since any frequency below 500 Hz has interference due to a large amount of ambient noise, which could interfere with the results and 5000 Hz was the maximum frequency possible with the sample rate of 10,000

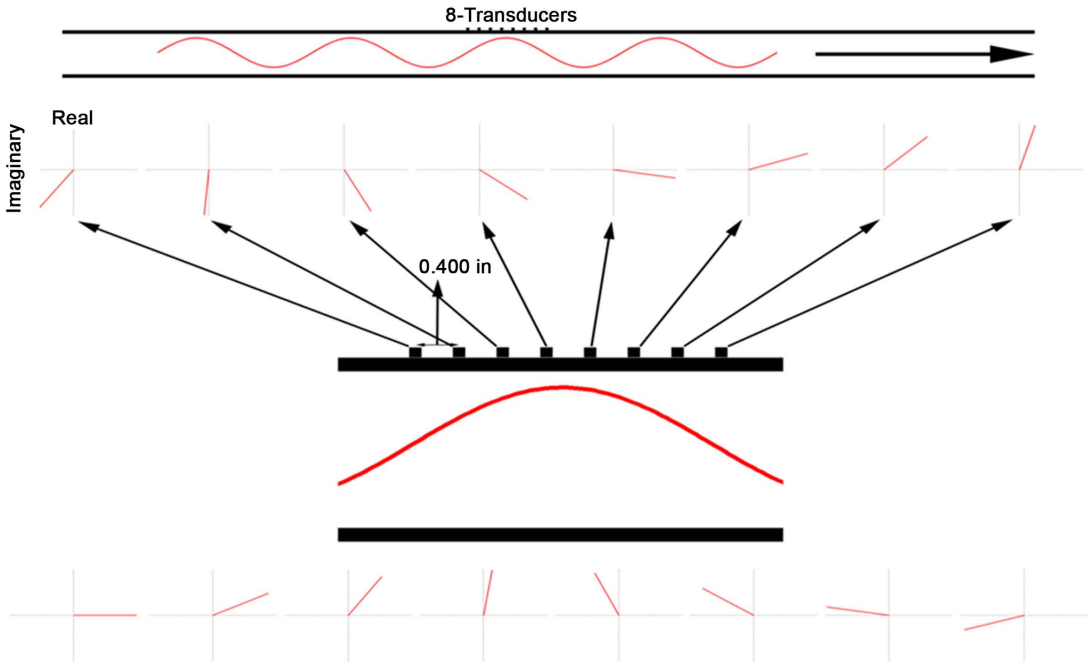

Figure 1. The acoustic array with 8 microphones.

samples/s due to the Nyquist limit. The sound wave was measured using 8 transducers 0.01016 m apart. Since the minimum frequency used was 500 Hz, the distance between the microphones needed to be larger than the maximum wavelength; thus, 0.01016 m (equivalent to 0.4 in) was chosen due to the precision of the machinery available. The 450 data points taken from the instrument were then converted using an analog-digital converter (ADC) as seen in the block diagram in **Figure 2**. In order to determine the real and imaginary components of the phase, a Fourier Analysis was conducted on the data obtained from experimentation. In order to obtain a value for the speed of sound, the phase was plotted versus the position and the slope was calculated (**Figure 2**). The speed of sound along with the correlation coefficients for all frequencies from 500 to 5000 Hz was then plotted.

4. Data and Results

While the results obtained from experimentation yield a high correlation coefficient between the phases of the sound wave and the position along the pipe, the value obtained for the speed of sound is incorrect even at correlation coefficients of 0.999. The proposed cross-correlation method for determining the speed of a sound wave propagating through a pipe has been proven invalid for its intended purposes.

5. Conclusions

Based on the data obtained from experimentation, the Cross-Correlation Phase Measurement Technique has proven itself an inaccurate method in determining the speed of a sound wave propagating through a pipe at various frequencies. Even with a consistently high correlation coefficient between the phases of the sound wave and the position along the pipe, across the range of tested frequencies, the calculated speed of sound was inaccurate at a majority of the points (**Figure 3**). As seen in **Figure 3**, the range of frequencies: 1797 Hz - 2197 Hz, has a correlation coefficient close to 1; however, the speed of sound measured in m/s has a range of values from 207.1 m/s to 634.6 m/s. The speed of sound in air at room temperature should be 343 m/s [4]. The correlation coefficient and the incorrect data suggest a flaw in the Cross-Correlation Measurement Technique. The flawed methodology behind this Cross-Correlation Phase Measurement Technique has neglected the presence of the reflected wave moving through the pipe in its calculations, thus resulting in inaccurate results. The inaccurate results are due to the superposition of the waves.

This technique does not take the superposition theory into account, but assumes that the input is coming from only one direction. Superposition of a sound wave describes a state of interference between multiple sound waves. This interference can be either constructive, where the waves are additive, or destructive, where the waves are reductive. This effect can be seen in the reflection of a sound wave in the pipe when two waves combine to form one superimposed sound wave. To illustrate the magnitude of effect superposition has on the results, consider the wave shown below:

$$\Psi = \cos\left(2\pi f\left(t - \frac{x}{c+v}\right)\right) + \left(f\left(t - \frac{x}{c+v}\right)\right) \tag{5}$$

where f is the frequency; c is the speed of sound; and v is the flow velocity, which adds to c when the flow velocity is in the same direction as the propagating wave. The equation assumes the presence of the same wave from another source, 90˚ out of phase with 1% amplitude of the above wave. The resulting wave would have

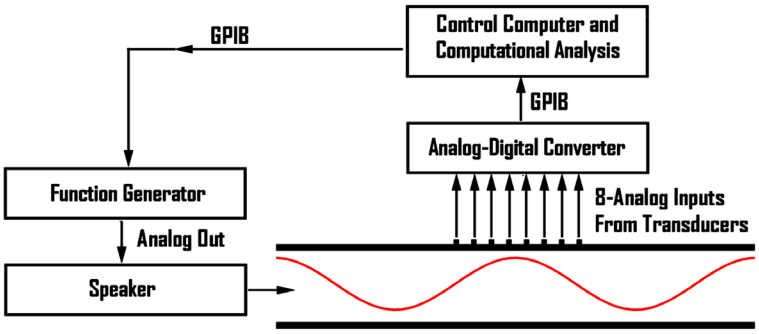

Figure 2. Block diagram of the experiment.

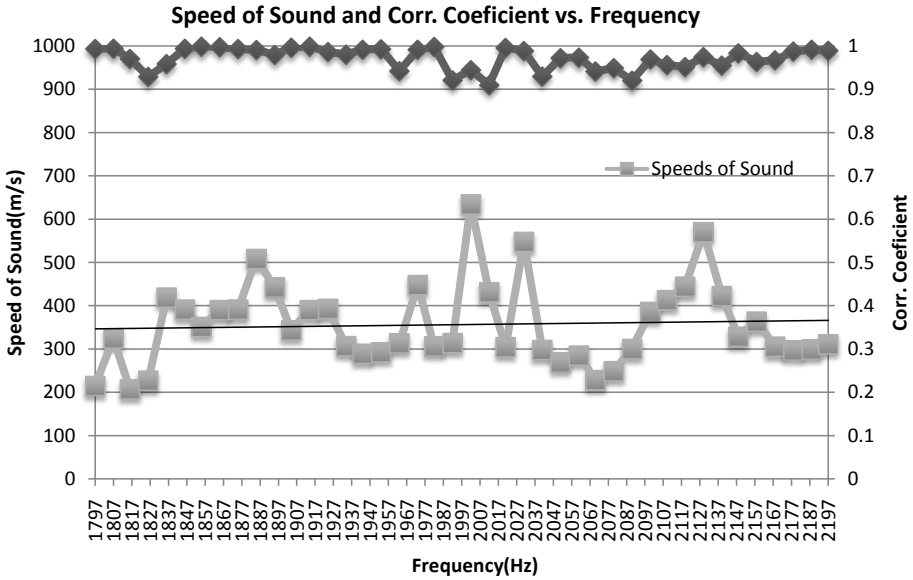

Figure 3. Speed of sound and correlation coefficient versus frequency.

a phase difference of 0.57 = $\tan^{-1}(0.01)$ or 0.16% full scale. While 0.16% may seem small, this slight discrepancy translates into a notable error of 0.56 m/s for a speed of sound of 350 m/s, and given a full range of flow velocity from 0 m/s to 10 m/s, it translates to 5.6% error in flow velocity.

To give an idea of magnitude by converting the interfering wave amplitude to the input wave amplitude, a 40 dB difference is revealed in sound. This is equivalent to the sound level in a library. It is very likely that noise of this level, or more, would be present from the ambient noise in the pipe or from reflected waves.

$$\frac{I}{I_o}=\left(\frac{\Delta A}{A}\right)^2=0.0001,\ \text{or}\ \ \beta=10\log\left(\frac{I}{I_o}\right)=-40\ \text{dB} \tag{6}$$

To employ acoustics to measure this phase phenomenon, it will be necessary to detect and separate out any miscellaneous background sound waves in order to more accurately analyze the sound wave present in the pipe. If the sound can be separated, it may be possible to use the ambient noise for the phase measure, and thereby remove the need for a sound source.

Acknowledgements

We would like to thank Georgia College and State University for providing the materials and space needed for this research.

References

[1] Kennedy, J.L. (1993) Oil and Gas Pipeline Fundamentals. 2nd Edition, PennWell Books, Oklahoma, 3-5.

[2] Beck, M.S. and Plaskowski, A. (1987) Cross Correlation Flowmeters, Their Design and Application. Taylor & Francis, UK.

[3] Taylor, J.R. (2005) Classical Mechanics. University Science Books, Sausalito, 688.

[4] Kirkpatrick, L. and Francis, G. (2010) Physics: A Conceptual World View. 7th Edition, Brooks/Cole, Cengage Learning, California, 331.

Call for Papers

Open Journal of Acoustics

ISSN 2162-5786 (Print) ISSN 2162-5794 (Online)
http://www.scirp.org/journal/oja

Open Journal of Acoustics (OJA) is an international journal dedicated to the latest advancement of acoustics. The goal of this journal is to provide a platform for scientists and academicians all over the world to promote, share, and discuss various new issues and developments in different areas of acoustics.

Editor-in-Chief

Editorial Board

Subject Coverage

This journal invites original research and review papers that address the following issues in acoustics. Topics of interest include, but are not limited to:

- Acoustic and Speech Signal Processing
- Acoustic Material
- Acoustic Measurement
- Acoustic Problems in Information Science
- Acoustic Signal Processing
- Acoustic Transducer, Acoustic Measurements and Methods
- Architectural Acoustics and Electroacoustics
- Fluid Dynamics and Acoustics
- Infrasonics
- Linear Acoustics
- Musical Acoustics
- Noise, Noise Effects and Control
- Nonlinear Acoustics
- Other Physical and Acoustic-Related Issues and Cross-Disciplinary
- Physical, Psychological Acoustics and Bioacoustics
- Sound of Water and Marine Acoustics
- Structural Acoustics and Vibration
- Ultrasonics in Medicine
- Ultrasonics, Quantum Acoustics and Acoustic Effects

We are also interested in short papers (letters) that clearly address a specific problem, and short survey or position papers that sketch the results or problems on a specific topic. Authors of selected short papers would be invited to write a regular paper on the same topic for future issues of the ***OJA***.

Notes for Intending Authors

Submitted papers should not have been previously published nor be currently under consideration for publication elsewhere. Paper submission will be handled electronically through the website. All papers are refereed through a peer review process. For more details about the submissions, please access the website.

Website and E-Mail

http://www.scirp.org/journal/oja **Email: oja@scirp.org**

What is SCIRP?

Scientific Research Publishing (SCIRP) is one of the largest Open Access journal publishers. It is currently publishing more than 200 open access, online, peer-reviewed journals covering a wide range of academic disciplines. SCIRP serves the worldwide academic communities and contributes to the progress and application of science with its publication.

What is Open Access?

All original research papers published by SCIRP are made freely and permanently accessible online immediately upon publication. To be able to provide open access journals, SCIRP defrays operation costs from authors and subscription charges only for its printed version. Open access publishing allows an immediate, worldwide, barrier-free, open access to the full text of research papers, which is in the best interests of the scientific community.

- High visibility for maximum global exposure with open access publishing model
- Rigorous peer review of research papers
- Prompt faster publication with less cost
- Guaranteed targeted, multidisciplinary audience

Scientific Research Publishing

Website: http://www.scirp.org

Subscription: sub@scirp.org

Advertisement: service@scirp.org